Pandemic *Vibrio parahaemolyticus* wave succession by gene loss

Chao Yang[1,#*], Hongling Qiu[2,#], Sarah L. Svensson[1#], Chengpei Ni[3,#], Song Gao[3], Zhizhou Jia[1], Huiqi Wen[1], Li Xie[1], Wenxuan Xu[1], Yujiao Qin[1], Shuzhu Lin[1], Jiancheng Wang[1], Yiquan Zhang[4], Yinghui Li[5], Min Jiang[5], Xiaolu Shi[5], Qinghua Hu[5], Zhemin Zhou[6], Yanjie Chao[1], Ruifu Yang[7], Yujun Cui[7], Jaime Martinez-Urtaza[8,*], Hui Wang[2,*], Daniel Falush[1,*]

[1] The Center for Microbes, Development and Health, CAS Key Laboratory of Molecular Virology and Immunology, Shanghai Institute of Immunity and Infection, Chinese Academy of Sciences, Shanghai, China;

[2] School of Public Health, Shanghai Jiao Tong University School of Medicine, Shanghai, China;

[3] Wuxi Center for Disease Control and Prevention, Wuxi, China;

[4] Department of Clinical Laboratory, Nantong Third People's Hospital, Affiliated Nantong Hospital 3 of Nantong University, Nantong, Jiangsu, China;

[5] Shenzhen Center for Disease Control and Prevention, Shenzhen, China;

[6] Key Laboratory of Alkene-Carbon Fibers-Based Technology & Application for Detection of Major Infectious Diseases, Cancer Institute, Suzhou Medical College, Soochow University, Suzhou, China;

[7] State Key Laboratory of Pathogen and Biosecurity, Academy of Military Medical Sciences, Beijing, China;

[8] Department of Genetics and Microbiology, Facultat de Biociències, Universitat Autònoma de Barcelona, Barcelona, Spain

# These authors contributed equally to the article

* Corresponding authors:

C.Y.: cyang@siii.cas.cn; J.M.-U.: Jaime.Martinez.Urtaza@uab.cat;

H.W.: huiwang@shsmu.edu.cn; D.F.: daniel.falush@siii.cas.cn

Abstract

While the importance of spontaneous mutation and gene acquisition in the emergence and adaptive evolution of microbial pathogens is well recognized, the role of gene loss remains underexplored. Here, by large-scale phylogenomic analysis of 8,684 global isolates, we reconstructed the origin and evolutionary dynamics of the pandemic clone (PC) of *Vibrio parahaemolyticus*, the leading cause of seafood-associated infections worldwide. As has also been observed for the pandemic lineage of *V. cholerae*, the emergence of the clone involved the acquisition of multiple marker genes and genomic islands within a short timeframe (~60 years), followed by divergence into distinct, successive sublineages mediating independent waves of cross-country transmission. In *V. parahaemolyticus*, a recent wave succession event within the last two decades has been driven by gene-loss in the putrescine utilization (Puu) pathway, which confers phenotypic advantages related to environmental adaptation (enhanced biofilms) and human transmission (increased cell adhesion and intestinal colonization, reduced virulence in an animal model and milder clinical symptoms in humans), aligning with the trade-off hypothesis of pathogen virulence evolution. We identify similar lineage-specific Puu-gene-loss across multiple bacterial genera, with effects on biofilm and adhesion replicated in *V. cholerae* and *Escherichia coli*, suggesting convergent evolution and universal phenotypic effects across bacteria. Our findings highlight the indispensable role of gene loss in the adaptive evolution of bacterial pathogens.

Introduction

Microbial pathogens have recurrently emerged from environments or animals, with a few leading to disease epidemics or pandemics that pose notable public health challenges[1,2]. Understanding the genetic basis of pathogen emergence and adaptive evolution is critical for disease control and prevention, especially for pandemic pathogens. *Vibrio*, Gram-negative, halophilic bacteria that are ubiquitous in marine and aquatic habitats, are ideal models for investigating pathogen emergence and evolution. Among >100 *Vibrio* species, approximately 12 cause human infections[3]. Two species, *V. cholerae* and *V. parahaemolyticus*, are associated with disease pandemics, with the ongoing seventh cholera pandemic attributed to El Tor (7PET) isolates. *V. cholerae* 7PET was inferred to originate from a pre-pandemic strain that subsequently underwent explosive diversification - gaining multiple genetic elements within a short timeframe (~15 years), including the El Tor type cholera toxin prophage and *Vibrio* seventh pandemic islands (VSP-I and VSP-II)[4,5]. During the seventh pandemic, three successive sub-lineages of 7PET were identified, corresponding to the three independent but overlapping waves of global transmission[5,6], which may be driven by antibiotic resistance[7].

V. parahaemolyticus is the leading cause of seafood associated infections worldwide, with an increase in incidence over the last two decades. Its geographical range has also been expanding, possibly due to global warming[3,8,9]. The emergence of pandemic clone (PC), characterized by serotype O3:K6, substantially changed the *V. parahaemolyticus* epidemiology[10–12]. The O3:K6 PC strain was first isolated in 1995 from a traveler returning to Japan from Indonesia, and in 1996, it caused a disease outbreak in Calcutta, India[10]. Subsequently, it rapidly spread worldwide and came to dominate infections in many regions, along with rapid antigenic divergence (49 serotypes reported)[10–12]. Molecular and

epidemiological surveillances has provided evidence that the PC may have originated from a serotype O3:K6 non-pathogenic strain, after acquisition of multiple marker genes (e.g. virulence regulatory gene sequence *toxRS/new*[13], phage f237 and its unique open reading frame *orf8*[14]) and marker genomic islands (VPaI-1 to VPaI-7), along with several virulence-associated loci such as those encoding Type 3 or 6 secretion systems (T3SS2 or T6SS1)[15,16]. However, how these events happened, the driving force and mechanism underlying these events remain unclear. Currently, there is a lack of comprehensive genomic view on the origin and evolution of the PC.

Leveraging a large-scale, global genome dataset of *V. parahaemolyticus*, which includes strains from six continents and 34 countries, we comprehensively reconstructed the evolutionary history of the PC. Intriguingly, we identified several similarities between PCs of *V. parahaemolyticus* and *V. cholerae*. However, distinct from *V. cholerae*, we demonstrated that gene-loss in the putrescine utilization pathway has driven the recent global wave succession event by conferring phenotypic advantages, and these phenotypic effects are likely universal among bacteria.

Results

From pre-pandemic (pre-PC) to PC

We assembled a total of 8,684 high-quality (completeness >90% and contamination <5%) genomes of global *V. parahaemolyticus* isolates, including 333 newly sequenced genomes (**Supplementary Table 1**). To characterize population structure and identify PC isolates, we constructed a maximum-likelihood (ML) phylogenetic tree based on core-genome single-nucleotide polymorphisms (SNPs). Based on the ML tree and pairwise SNP-distance, 2,815 were assigned as PC isolates (mean SNP-distance: 437), 39 as pre-PC (close relatives of PC, mean SNP-distance to PC: 15,463), with the remaining being non-PC isolates (mean SNP-distance to PC: 55,554, **Fig. 1a**).

Pre-PC isolates were further split into four sub-groups, designated pre-PC1 to pre-PC4, respectively (**Fig. 1b,c**). Pre-PC1 to pre-PC3 were exclusively identified in Asia, with pre-PC1 and pre-PC2 being clinical isolates, while pre-PC3 were mainly environmental strains. The closest relative of the PC, pre-PC4, was represented mainly (13/16) by environmental isolates from Asia (Japan and China) and the US. The serotypes of most pre-PC isolates (33/39) were predicted to be O3:K6, and sequence types (STs) of pre-PC4b (a subset of pre-PC4) isolates were ST3 except one strain (**Fig. 1c** and **Supplementary Table 2**).

Among Pre-PC and PC isolates, we identified a total of 88,754 core-genome SNPs, with 94% attributed to homologous recombination, suggesting that recombination was the primary driver of divergence from pre-PC to PC. We further assessed the temporal signal using the ML tree based on recombination-stripped SNPs and strain isolation dates. A significant signal (p<0.01) was detected among strains from pre-PC3b to PC, allowing inference of the dated phylogeny (**Fig. 1b,2b**). The most recent common ancestor (MRCA) of the PC was estimated at 1983 (95% confidence interval [CI]: 1979-1985), 12 years preceding its first discovery in 1995. The strains are expected to be highly homogeneous at the point of their origin, but early

PC strains from 1996 already showed some diversity (an average of 38 non-recombined SNPs), consistent with the long time-interval between their origination and first discovery (**Fig. 2b**).

We investigated the distribution of known PC marker genes/islands and inferred the evolutionary history from pre-PC to PC (**Fig. 1b,c** and **Extended Data Fig. 1)**. The PC likely originated from a serotype O3:K6 pathogenic strain encoding T3SS1, T6SS2, phage f237 and VPaI-3, and subsequently acquired T6SS1 and the *toxRS/new* sequence. Between 1920 (MRCA of pre-PC4b and PC) and 1983 (MRCA-PC), MRCA-PC gained multiple known marker genes/islands distributed across distinct genomic loci, including *orf8* and six out of the seven VPaIs, as well as the gene encoding the well-known virulence factor thermostable direct hemolysin, *tdh.* Additionally, 86 point mutations (34 synonymous; 38 non-synonymous) and 80 homologous recombination events (524 kb, 10% of the reference genome) were inferred along this branch. Moreover, *trh* (*tdh*-related hemolysin), VPaI-1 and VPaI-2 were independently gained or lost by pre-PC strains.

We further investigated the source of these marker genes/islands by searching against non-PC genomes. All of them were identified in non-PC isolates, although at low frequency **(Fig. 1c**, **Extended Data Fig. 2**), indicating that these elements are more likely the result of intra-species transfer from diverse non-PC *V. parahaemolyticus* strains than of cross-species transfer from other *Vibrio* or bacterial species. Moreover, the differing distribution patterns of these marker genes/islands among pre-PC and PC strains suggest that they were unlikely to have been acquired simultaneously in a single burst. Apart from marker genes/islands, six PC-specific genes were identified, three of which were within the superintegron (**Supplementary Table 3**).

Fine-scale population structure of PC

To reduce the effect of repeat sampling (strains from disease outbreaks) and exclude outlier strains, we generated a representative subset of 942 PC isolates for further analysis (see methods), spanning 20 countries across five continents isolated between 1996 and 2022 (**Extended Data Fig. 3**). Among the representative isolates, we identified 26,377 core-genome SNPs, with 66% attributed to homologous recombination. Two recombination hotspots were identified, including the known O:K antigen region[17] and a novel hotspot (VP1883-1891) encoding a type II toxin-antitoxin system and a cold shock protein. There were 281 homoplastic non-recombined SNPs, of which 26 were convergently identified 6-18 times in 16 genes associated with quorum sensing, environmental response and virulence (**Extended Data Fig. 4** and **Supplementary Table 4**).

We constructed an ML tree and dated phylogeny for PC representative strains (**Fig. 2a,b**). By integration with hierarchical clustering (**Extended Data Fig. 5**), we split the PC into four sub-lineages corresponding to independent waves of cross-country transmission (**Fig. 2a-d**), which was also observed in the *V. cholerae* 7PET[5]. Following the nomenclature of *V. cholerae*, we designated these sub-lineages as wave-1 to 4, respectively. The estimated MRCA times for wave-1 to wave-3 were close (1984-1987), while wave-4 emerged more recently in 1998.

We identified 11 serotypes and three STs in representative strains (**Fig. 2b**). While O3:K6 was dominant (79%), serotype conversions were identified, particularly in wave-2 and wave-3. ST3 (96%) remained the predominant ST. Several marker genes/islands (VPaI-1, 4, 5 and *orf8*) were lost in 2%-8% of representative isolates, with the others being conserved (**Extended Data Fig. 6a**). Notably, the genomic island VPaI-7, which encodes *tdh* and T3SS2, showed high differentiation between different waves (**Extended Data Fig. 6b**). Additionally, we observed a conserved antimicrobial resistance (AMR) gene profile (**Extended Data Fig. 6a**). Apart from intrinsic ampicillin resistance-related genes, no recently acquired gene was identified in >1% of representative isolates.

Wave succession and global transmission

Remarkably, we identified a clear 'wave succession' pattern: wave-1 to wave-4 succeeded each other temporally as the major wave in China, where sampling is sufficient. Similar trends were also seen in other countries with ≥10 representative strains, including the US, UK, Canada and Bangladesh, suggesting a possible global pattern. In contrast, in two South American countries, Peru and Chile, wave-1 has remained dominant for over a decade (**Fig. 2c,d**).

Wave-4 frequency has been increasing since its emergence, ultimately becoming predominant from 2012 onward. Since its origin, the effective population size (N_e) of the PC increased exponentially until 1998 (**Fig. 2e**). Subsequently, N_e fluctuated and showed a decreasing trend after 2010. Population dynamics of waves was consistent with temporal dynamics, with the N_e peaking alternatively for different waves. Post-2010, the N_e of wave-4 exceeded others and remained stable, while N_e of other waves declined rapidly.

We inferred the geographical transmission history of the PC by phylogeographical analysis, focusing on cross-continent events. A total of 67 transmission events were identified, mostly transient and not leading to local colonization (**Extended Data Fig. 7**). Only six 'TC' events (Transmissions resulting in local Colonization that persisted for ≥3 years) were identified (**Fig. 2b** and **Extended Data Fig. 7**). Wave-1 in South America likely sourced from a single TC event from Asia to Peru in 1990 (TC1), much earlier than its first discovery in South America (1997). Subsequently, wave-1 spread from Peru to Chile and backward transmissions were also identified (TC2-4). Additionally, two TC events from Asia to North America were identified (TC5-6) in other waves.

Puu-gene loss is associated with wave-4 replacement

To investigate the genetic basis of the wave-4 replacement of other waves, we comprehensively identified wave-4-specific variations and examined their functions. A total of 40 variations were identified (**Fig. 3a** and **Extended Data Table 1**), including 29 SNPs (located in 26 genes and 3 intergenic regions), two small indels (located in 2 genes) and most notably, the absence of nine adjacent genes (VP1775-VP1786). Of the nine genes, five are annotated as part of the putrescine utilization (Puu, VP1775-1781) pathway, one encodes a Na^+/H^+ antiporter (VP1782), and the others encode hypothetical or DUF3291

domain-containing proteins (VP1783-1786).

The fixation of gene loss is expected to be adaptive and selection-driven in free-living species, which are generally believed to have large N_e[18]. Moreover, *Vibrio* species, which are abundant in marine environments, have been broadly estimated to exhibit large N_e[19]. Therefore, we hypothesize that the fixation of Puu-pathway gene loss in *V. parahaemolyticus* confers phenotypic advantages.

The enzymes encoded by Puu-pathway genes degrade the polyamine putrescine into 4-aminobutanoate (GABA) or spermidine (**Fig. 3b**). Specifically, the *puuC* gene is involved in three sub-pathways in the conversion of putrescine to GABA, and its deletion is expected to completely block this conversion, mimicking the effect of a complete deletion of Puu-genes **(Fig. 3b)**. Therefore, we generated a *puuC* deletion mutant in the wildtype strain RIMD2210633 (wave-3, hereafter RIMD-W3) to explore the function and consequences of loss of Puu-genes in *V. parahaemolyticus*.

Phenotypic effects of Puu-gene loss

Biofilm formation

We first tested the phenotypic effects of Puu-gene loss on biofilm formation, as the Puu-pathway has been reported to be involved biofilm formation in *Pseudomonas aeruginosa*[20]. As reported in *P. aeruginosa*, Δ*puuC* showed significantly (p<0.01) enhanced biofilm formation under M9 minimal media after 48 hours of culture (**Fig. 3c**), while complementation of the deletion strains *in trans* (C-Δ*puuC*) significantly decreased biofilm formation.

We next performed transcriptomic sequencing to identify differentially expressed genes (DEGs) that may underlie the increased biofilm of Δ*puuC*, as well as to explore other Puu-gene-loss related phenotypes. In line with increased biofilm formation of Δ*puuC*, we identified multiple DEGs between wildtype and Δ*puuC* associated with biofilm or biofilm-related pathways, including c-di-GMP and quorum sensing (**Fig. 3d, Supplementary Table 5**). We next quantified intracellular c-di-GMP levels in wildtype and Δ*puuC* during growth by introducing dual-fluorescence reporter plasmids. Consistent with differential expression of several c-di-GMP-related enzymes and higher biofilm formation, c-di-GMP levels were significantly higher in Δ*puuC* compared to wildtype in stationary phase (**Fig. 3e**).

Cell adhesion and intestinal colonization

The DEGs analysis give clues on the effects of Puu-gene-loss on other phenotypes in addition to biofiom. Specifically, the most significant category of DEGs (Δ*puuC vs.* RIMD-W3) were genes encoding CupE-fimbriae and Flp-pili (**Fig. 3d)**, which are generally related to cell adhesion for pathogens[21]. Motivated by these observations, we performed Caco-2 cell adhesion assays and found significantly enhanced adhesion for Δ*puuC* compared to wildtype (**Fig. 3f**). We also tested whether increased cell adhesion might transform into enhanced intestinal colonization. We constructed bioluminescent wildtype and Δ*puuC* strains and traced their colonization of mice after oral gavage using *in vivo* imaging. At 5 hours post-infection,

mice infected with Δ*puuC* exhibited stronger luminescence compared to wildtype (**Fig. 3g**). Bacteria were then rapidly cleared, with no detectable luminescence observed for both wildtype and mutant strains by 10 hours post-infection.

Virulence

An unexpected observation was the downregulation of the key virulence gene, *tdh*, in Δ*puuC* (2.6-fold, *p*-adj=0.02, **Fig. 3d**), suggesting that Puu-gene-loss might reduce virulence. Accordingly, we compared the lethality of wildtype and Δ*puuC* mutant strains in mice following intraperitoneal infection. Consistent with *tdh* downregulation, Δ*puuC* exhibited reduced lethality (**Fig. 3h**). These findings together revealed the potential impact of Puu-gene-loss on phenotypes related to human infection, including cell adhesion, intestinal colonization and virulence.

Phenotypes of wave-4 strains

The phenotypic experiments above provide clues about the selective advantages of wave-4 strains. To link the phenotypes related to Puu-gene-loss observed in a Δ*puuC* wave-3 strain with the behavior of natural wave-4 strains, we next compared 12 natural strains, including six wave-1 to wave-3 (2 strains each) and six wave-4 strains, for the same phenotypes as described above. Consistent with the above phenotypic differences between wildtype and mutant strains established above, the wave-4 strains exhibited enhanced biofilms and cell adhesion, compared with wave-1 to wave-3 strains (**Fig. 4a**). Moreover, we complemented a wave-4 strain (VPCZ58) with the nine genes (VP1775-VP1786) that are absent in wave-4 strains and identified significantly reduced biofilm formation and adhesion compared to the wildtype strain (**Fig. 4b**), providing further evidence that the Puu-genes are responsible for the observed phenotypic differences.

Additionally, we analyzed the clinical symptom data of 1,966 PC-related patients reported in our previous study[22], and found that wave-4 was associated with milder symptoms, including significantly lower rates of fever, vomiting and abdominal pain (**Fig. 4c**), consistent with reduced virulence observed in our mouse infection experiment (**Fig. 3h**).

We hypothesized that these phenotypic differences mediated by Puu-gene-loss might confer competitive advantages of wave-4 strains in the environment. Therefore, we performed competition experiments for natural strains in seawater with chitin as a nutrition source, mimicking a possible natural environment. We mixed wave-4 strains with those from other waves in equal (1:1) or different (1:5) ratios. By targeted PCR amplification of a gene with a wave-4-specific SNP allele (VPA0427 A919G), we quantified the relative abundance of wave-4 based on the frequency of the wave-4-specific allele. After 72 hours of competition, we measured a significant increase in the frequency of wave-4-specific alleles for both mixing ratios (**Fig. 4d**), demonstrating the competitive advantage of wave-4 under the tested condition.

Puu-gene-loss in bacteria

The convergent loss of Puu-genes and/or its fixation in specific bacterial lineages would

provide evidence supporting selection as the driving force. We analyzed the prevalence of Puu-genes among 108,526 genomes from 36 bacterial species, including *Vibrio*, common pathogens, and probiotics. Puu-genes were generally not conserved among bacteria, with part of the pathway lost in some species (**Fig. 5** and **Extended Data Table 2**). Notably, the absence/pseudogenization of Puu-genes in a subset of strains within species was convergently identified across multiple species (**Fig. 5b** and **Extended Data Fig. 8**). Furthermore, this absence/pseudogenization was fixed or nearly fixed in a specific lineage for species such as *Escherichia coli*, *Shigella boydii*, *S. sonnei* and *P. aeruginosa*, or convergently occurred in two or more lineages among species such as *Campylobacter coli*, *Yersinia pestis*, *Bifidobacterium longum* and *Lactobacillus helveticus.* Additionally, Puu-gene-loss was not only identified among *V. parahaemolyticus* PC strains, but also identified in the *V. cholerae* 7PET **(Fig. 5b)**.

To test if Puu-gene-loss has a similar phenotypic effect in other bacteria, we generated *puuC* deletion strains in *V. cholerae* (E7946 background) and *E. coli* (MG1655 background) and tested their biofilm formation and cell adhesion abilities. Consistent with the results in *V. parahaemolyticus*, the Δ*puuC* mutant strains in both species exhibited significantly enhanced biofilms and adhesion compared to their parental wildtype strains (**Fig. 5b**). Together, these results indicate that Puu-gene-loss is under selection in some species, and that the associated phenotypic consequences are potentially universal across bacterial species.

Discussion

Leveraging a large-scale genome dataset of global isolates, we present the most comprehensive genomic view to date on the origin and evolution of the *V. parahaemolyticus* PC. Our findings suggest that the PC likely originated from a serotype O3:K6 pathogenic strain through gain of multiple genes/islands within a short timeframe (~60 years) from *V. parahaemolyticus*, rather than from non-pathogenic strains or from other *Vibrio* species[11]. Notably, several characteristics previously considered to be specific to the PC[10–12], including ST3, *toxRS*/new, and VPaI-1 to VPaI-3, were also present in pre-PC strains, while the *orf8* gene remained unique to the PC, thus remaining as a reliable marker. Moreover, we described the fine-scale population structure and spatiotemporal dynamics of the PC, and identified 'wave succession' with potential underlying molecular mechanisms. Together, our findings substantially enhance the current understanding of how epidemic lineages of *V. parahaemolyticus* emerge and evolve.

During the evolution of the *V. parahaemolyticus* PC, we observed intriguing parallels with the *V. cholerae* 7PET strains and other pathogens. First, we observed gain of genes/islands, including key virulence genes (*tdh* and *ctxAB*) and marker genomic islands (six VPaIs and two VSPs) for the *V. parahaemolyticus* PC, as has been reported for the *V. cholerae* 7PET[4,5]. This phenomenon has also been observed during human colonization by other pathogens[23] and in the evolution of metabolic pathways across prokaryotic lineages[24]. Frequent human-mediated cross-regional transmission and adaptation to new environments are considered potential drivers for the *V. cholerae* 7PET[4], which might also apply to the *V. parahaemolyticus* PC. Second, for both PCs from pandemic *Vibrio* species, the inferred times

of origin (1983 and 1955[4]) and introduction to specific geographical regions (e.g. South America: 1990 and 1989[25]) were much earlier than their first epidemiological observations (1995 and 1961; South America: 1997 and 1991). Three possible explanations for this include inadequate surveillance, variability in the molecular clock rate[26] with higher early mutation rates[27,28], and the possibility of early cryptic disease epidemics, with specific events such as El Niño or warming in coastal conditions triggering a sudden surge in cases and thereby drawing epidemiological attention. While the third explanation does not apply to *V. cholerae* due to the high risk and strict surveillance of cholera, all explanations are applicable to *V. parahaemolyticus*. Third, divergence into successive sublineages mediating waves of infections, identified in both pandemic *Vibrio* and other pathogens such as SARS-CoV-2[29]. While antimicrobial resistance likely drove the wave succession of *V. cholerae* 7PET[7], *V. parahaemolyticus* exhibits low resistance rates to first-line antibiotics, indicating a different driving factor.

The importance of biofilm formation in bacterial environmental adaptation and survival under adverse conditions (e.g. antibiotic exposure) is well recognized[30]. Therefore, the enhanced biofilms mediated by Puu-gene-loss may improve the environmental adaptability of wave-4 strains, as suggested by our competition experiment results. Moreover, the ancestral strains of the PC, as well as most non-PC strains, carry the complete Puu-pathway genes, indicating that the loss of Puu-genes occurred recently, possibly in response to environmental changes. Putrescine serves multiple physiological functions in diverse organisms, including roles in cell growth and proliferation[31], and has been particularly reported to promote acid stress tolerance[32,33]. The loss of Puu-genes might have been selected for by recent increases in ocean or coastal acidification.

Human activities are pivotal in pathogen transmission. Increased cell adhesion and intestinal colonization could directly facilitate human-mediated transmission, while reduced virulence, associated with milder clinical symptoms, may lower the likelihood of seeking medical attention, thereby promoting cryptic transmission. Notably, increased adhesion and colonization are not contradictory to reduced virulence, as different infection routes in the experiments (gavage *vs.* intraperitoneal injection) and their underlying mechanisms are known to differ[34].

The effect of the Puu-pathway on biofilms is likely a broader phenomenon among bacteria than previously recognized. We have demonstrated that Puu-gene-loss enhances biofilms in three different species. Furthermore, Puu-gene-loss in *P. aeruginosa* also leads to enhanced biofilms[20], and *E. coli* phylogroup B2, characterized by absence of *puuA-D* (**Fig. 5b**) exhibits a stronger biofilm-formation ability than other phylogroups[35,36], providing further evidence for a more universal effect.

For the first time, we have established links between Puu-gene-loss, cell adhesion and intestinal colonization, which are also likely universal across bacteria. We demonstrated that Puu-gene-loss enhances cell adhesion in three different species and promotes intestinal colonization in *V. parahaemolyticus.* Furthermore, *E. coli* phylogroup B2 strains are often

associated with urinary tract infections[37] and show increased persistence in the intestines of human infants[38], both of which is consistent with the hypothesis of increased adhesion and colonization mediated by Puu-gene-loss. Interestingly, the probiotic *E. coli* strain Nissle 1917, known for its strong capability of human gut colonization[39], belongs to phylogroup B2 and lacks Puu-genes (**Fig. 5b**).

The convergent loss or pseudogenization of Puu-gene within species (e.g., *C. coli*) and across different bacterial species, along with its lineage-specific fixation (e.g., in *E. coli*), indicate that these events are more likely selection-driven in these species and may confer fitness advantages. Puu-gene loss/pseudogenization was uniquely fixed in major pathogenic clonal complexes (CC) of *S. boydii* (CC145) and *S. sonnei* (CC152)[40], and recently fixed in *V. parahaemolyticus* wave-4, suggesting potential fitness advantages for human infection or transmission. However, this appears to not always be the case, as Puu-gene loss/pseudogenization has not occurred in major pathogenic lineages of *C. coli* and *P. aeruginosa*. Additionally, Puu-gene loss/pseudogenization appears to be associated with lineage divergence in *E. coli* and *C. coli*, and Puu-gene gain is potentially linked to human adaptation in the probiotic *B. longum*, with Puu-genes predominantly identified in adult human strains and absent in infant or non-human strains. These observations together indicate that while Puu-gene loss/pseudogenization is likely selection-driven in some species, the underlying driving forces vary across different species.

While the significance of spontaneous mutation and gene acquisition in pathogen evolution is well recognized[41–43], the role of gene loss remains underexplored. Gene loss is pervasive across all life kingdoms[44,45]. In bacteria, it is commonly observed in symbionts and host-dependent pathogens, where is generally considered neutral and driven by genetic drift associated with transmission bottleneck[46,47], while loss of several specific genes has been experimentally validated to be associated with pathogen virulence[48–50]. Notably, gene loss affecting polyamine metabolism has also been reported in the pathogen *Shigella*, where the polyamine cadaverine was found to inhibit enterotoxin activity[48]. This aligns with our findings in *V. parahaemolyticus*, in which elevated levels of a different polyamine, putrescine, are associated with reduced virulence. Together, these findings suggest a potentially broader role for polyamines (e.g., cadaverine and putrescine) in modulating bacterial pathogenesis.

Free-living bacteria with a large N_e serve as better models for investigating adaptive evolution driven by gene loss, as such fixation is more likely to be adaptative and selection-driven. Some free-living bacteria, such as the abundant open-ocean bacterioplankton *Prochlorococcus*, exhibit extensive gene loss, which has been attributed to accelerated evolution and fitness advantages conferred by genomic and metabolic "streamlining"[51,52]. Moreover, previous studies of gene loss-mediated bacterial adaptation, whether for symbionts, host-dependent pathogens, or free-living species, generally come with the cost of transition from generalists capable of surviving in diverse environments to specialists adapted to specific ecological niches[49–52]. The exact niche of the *V. parahaemolyticus* PC remains unclear but it is more likely a generalist due to widespread distribution in marine and aquatic habitats. If we consider different geographical regions as the macro-niches, the wave-4 strains

characterized by Puu-gene-loss have spread globally, without clear evidence supporting its transition from a generalist to specialist strategy. Therefore, our study presents a novel pattern of gene loss-mediated adaptation in free-living species.

In summary, our study provides the most comprehensive genomic view on the origin and evolution of the *V. parahaemolyticus* PC. We identified several interesting common features between the evolution of pandemic clones in two *Vibrio* species, but the driving forces underlying wave succession events appear distinct. While spontaneous mutation and gene gain-mediated antibiotic resistance may drive the *V. cholerae* 7PET succession[7], we demonstrated that Puu-gene loss, which confers phenotypic advantages related to environmental adaptation and human transmission, has likely driven the recent *V. parahaemolyticus* wave succession. An interesting finding is that *V. parahaemolyticus* wave succession has come along with reduced virulence, which aligns with the trade-off hypothesis of pathogen virulence evolution[53]. We also found that Puu-gene-loss is general and frequent among bacteria, selection-driven in multiple species, with its phenotypic impacts likely universal across species. Furthermore, Puu-gene-loss may play key roles in bacterial evolution, including lineage divergence (e.g. *E. coli*, *C. coli* and *B. longum*), human adaptation (e.g. *B. longum*) and the epidemic expansion of specific pathogenic lineages (e.g. *V. parahaemolyticus*, *S. boydii* and *S. sonnei*). Taken together, our study underscores the indispensable role of gene loss in the adaptative evolution of bacterial pathogens.

Methods

V. parahaemolyticus genome dataset

A total of 8,684 high-quality genomes were included in this study, including 333 newly sequenced and 8,351 publicly available genomes (**Supplementary Table 1**). Public genomes (up to November 2022) were downloaded from National Center for Biotechnology Information GenBank or Sequence Read Archive (SRA) database, with metadata extracted from corresponding BioSample information or the literature. New genomes were obtained from archived strains isolated from multiple countries, including China, Japan, Senegal, Peru and Chile.

Whole genome sequencing of new strains was performed using Illumina NovaSeq or Miseq platforms. New and public sequencing reads were trimmed using Trimmomatic v0.39[54] and were *de novo* assembled using shovill v1.1.0 pipeline (https://github.com/tseemann/shovill). The quality assessment of genomes was performed using CheckM v1.1.3[55]. Whole genome average nucleotide identity (ANI) against the reference genome of *V. parahaemolyticus* (RIMD2210633, accession numbers: NC_004603.1 and NC_004605.1) was calculated using fastANI v1.1[56]. Only high-quality genomes (completeness >90% or contamination <5%) with ANI >95% were included in further analysis.

Phylogenetic and phylogeographical analysis

Genome sequences were aligned against the reference genome using MUMmer v3.23[57] to generate whole-genome alignments. Core-genome (regions present in >99% strains) single-nucleotide polymorphisms (SNPs) were identified using SNP-sites v2.5.1[58]. SNPs

located in repetitive regions identified by TRF v4.07b[59] or BLASTN self-search were excluded. Non-repetitive SNPs were used to construct maximum-likelihood (ML) phylogenetic trees using FastTree v2.1.10[60] for all the isolates.

For both pre-PC and PC strains, recombination regions and associated length were detected using Gubbins v3.1.3[61]. Homoplastic SNPs and nutations (non-recombined SNPs) along the phylogenetic branch were identified using SNPPar v1.0[62] based on ancestral state reconstruction of these variations. Non-recombined and non-homoplastic SNPs were used for the construction of ML tree using RAxML-NG v1.0.1[63] with the GTR+Γ model. Phylogenetic trees were visualized using ggtree[64]. Hierarchical clustering analysis were performed using fastBAPS v1.0.6[65] to assign strains into subgroups. The transitions in the isolation countries of strains in the phylogenetic tree are considered cross-country events. These were identified manually, and all events are shown in detail in Extended Data Fig. 7. TC was defined as Transmissions resulting in local Colonization (persisted for ≥3 years).

Temporal analysis and population size dynamics

Temporal signals among pre-PC and PC isolates were assessed based on the recombination-stripped ML tree using TempEst v1.5.3[66], by calculating the correlation between root-to-tip distances and strain isolation dates (years). A significant temporal signal was detected among strains from pre-PC3b to PC ($p<0.01$, $R=0.62$), whereas inclusion of pre-PC3a and earlier pre-PC strains eliminated the significant signal. A significant temporal signal was also detected within PC strains alone ($p<0.01$, $R=0.57$). For strains showing a significant temporal signal, we applied BactDating v1.1.0[67] to infer the dated phylogenetic trees with the additive relaxed clock (ARC) model. The effective sample sizes (ESS) of the estimated parameters were all above 200. Effective population size dynamics was inferred using skygrowth v0.3.1[68] based on dated trees with default parameters.

Serotype and MLST typing

In silico O- and K-antigen genotyping was performed using the *V. parahaemolyticus* Kaptive database[69]. Multi-locus sequence typing (MLST) was performed using mlst (https://github.com/tseemann/mlst) to scan genome sequences against the PubMLST databases.

Representative genome dataset of PC

We generated a representative subset of 942 PC isolates. First, to reduce the effect of repeat sampling such as strains from disease outbreaks, we selected the genome with maximum N50 from a cluster of strains with ≤6 SNPs from same country and within a year, representing putative outbreaks[22]. Second, we calculated root-to-tip distances of phylogenetic trees based on non-recombined SNPs, and removed putative hypermutators with extreme root-to-tip distances and branch lengths (**Extended Data Fig. 3**).

Core-pangenome

All PC representative genomes were re-annotated using Prokka v1.13[70], and the annotation outputs (GFF3 files) were used in Panaroo v1.2.8[71] to identify the core-pangenome and gene

presence/absence.

Wave-4 specific variations

We analyzed three types of variations, including SNPs, gene presence/absence and unitigs. The SNPs and gene presence/absence data were extracted from the preceding analysis. The unitig matrix was determined using unitig-caller v1.2.1 (https://github.com/bacpop/unitig-caller). Unitig sequences were aligned against assembled genomes using BLASTN to identify corresponding genomic positions and related genes. Wave-4 specific variations were defined as alleles, genes or unitigs present/absent in >95% of wave-4 strains and <5% of non-wave-4 strains.

***puuC* gene in the reference genome**

The *puuC* gene (VP_RS08540/VP1776-7) in the reference genome RIMD2210633 was annotated as a pseudogene due to a frameshift caused by insertion of one nucleotide within a homopolymeric region (three consecutive adenines). However, we performed both Sanger sequencing and Illumina re-sequencing of this region in our RIMD2210633 strain. Both sequencing methods confirmed absence of this nucleotide and an intact *puuC* ORF in our strain, with no frameshift detected. Given the low sequencing depth of the original reference genome (average 8.9×) and the elevated error rate associated with homopolymeric regions, we hypothesize that the frameshift reported in the reference genome is likely caused by a sequencing error.

Puu-genes in bacteria

We investigated the prevalence of Puu-genes in 36 bacterial species, including *Vibrio*, common pathogens, and probiotics. We included a total of 108,526 genomes (62-24,205 genomes per species, **Supplementary Table 6**) downloaded from Genome Taxonomy Database (GTDB, release207)[72]. Puu-related protein sequences in *E. coli*, *P. aeruginosa* and *V. parahaemolyticus* were used as initial queries, which were searched against all genomes of the selected 36 species using TBLASTN to identify the reference genes of each species (**Extended Data Table 2**). Nucleotide and protein sequences of the reference genes for each species were then searched against all genomes of the corresponding species using BLASTN and TBLASTN. We combined BLASTN and TBLASTN results to identify the presence, absence or pseudogenization of genes, with identify >80% and coverage >70% as cutoffs. A gene was classified as present if a BLASTN or TBLASTN match was identified. If only a BLASTN match was identified, the gene was classified as a pseudogene; otherwise, it was considered absent.

Bacterial strains and growth conditions

A total of 12 *V. parahaemolyticus* representative strains (pairwise SNP distances: >6) were used for laboratory experiments, including reference strain RIMD2210633 (wave-3) and 11 previously or newly sequenced PC strains. Additionally, *V. cholerae* strain E7946 (El Tor, Ogawa) and *E. coli* strain MG1655 (K12) were included. We chose *E. coli* and *V. cholerae* for two main reasons: our detection of natural strains with Puu-gene loss, and the availability of strains in our laboratory. In addition, *V. cholerae* is another *Vibrio* species associated with

disease pandemics, and *E. coli* is a widely used model organism. *V. parahaemolyticus* strains were grown routinely in rich broth (LB with 3% NaCl) with shaking or on agar plates at 30°C aerobically. *E. coli* and *V. cholerae* strains were cultured in LB at 37°C.

Mutant construction

Deletion mutants of *V. parahaemolyticus* were constructed by homologous recombination and counterselection with the suicide plasmid pDM4 as previously described[73], with 1kb of homology upstream and downstream of the desired mutation. For *V. cholerae*, a similar approach with pDM4 was used as for *V. parahaemolyticus*, except *E. coli* MFD*pir* was used as donor strain for conjugation. *E. coli* deletion mutants were constructed using λ red recombination as previously described[74]. *V. parahaemolyticus* deletion strains were complemented with the corresponding gene *in trans* on plasmid pMMB207 using the Ptac promoter. All deletion and complement clones were verified by colony PCR. All constructed strains and plasmids are listed in **Supplementary Table 7**.

Biofilm assays

Log-phase cultures were inoculated into M9 medium with 1% NaCl in 96-well plates (Kingmorn biotechnology) and incubated under static conditions at 37°C for 48 hours. Following incubation, culture medium was discarded, and 96-well plates were washed with 0.9% NaCl twice, dried at 60 °C for 30 min, and stained with 100 μl 0.1% (w/v) crystal violet solution for 10 min. After staining, the plates were washed with 0.9% NaCl three times. The bound crystal violet was resolubilized with 100 μl 95% ethanol for 10 min and quantified via OD_{595} with BioTek Synergy H1 (Agilent Technologies). Each strain was tested with 30 technical replicates.

RNA extraction and transcriptome analysis

Strains were grown to stationary phase in M9 medium with 1% NaCl and harvested after treatment with stop mix (5% phenol, 95% ethanol). Total RNA was extracted from cells using the hot-phenol method as described previously[75]. RNA was DNase I-digested and rRNA depleted. cDNA libraries were constructed at Novogene Co. Ltd. (Beijing, China) and sequenced on an Illumina NovaSeq platform.

Sequencing reads were trimmed using Trimmomatic v0.39[54] and then mapped to the reference genome using BWA v0.7.17[76]. The number of reads assigned to genes were counted using featureCounts v2.0.6[77]. Differentially expressed genes and pathway enrichment analysis were performed using R packages DESeq2 v1.34.0[78] and ClusterProfiler v4.2.2[79].

c-di-GMP assay

To measure intracellular c-di-GMP, we used a previously published riboswitch-based reporter system[80]. Log-phase cultures of strains carrying the reporter were inoculated into M9 medium with 1% NaCl and 50 μg/ml spectinomycin in 96-well plates (six replicate wells per strain). Additionally, six wells of blank control with 200 μl uninoculated medium were included. The plate was incubated in a BioTek Synergy H1 plate reader (Agilent Technologies) at 37°C for 48 hours. OD_{600} and fluorescence (455 nm excitation/489 nm emission for AmCyan and 540

nm excitation/574 nm emission for TurboRFP) were measured every 15 min. The average values of the control wells were subtracted from each measurement (OD_{600}, AmCyan, and TurboRFP) of the strains. The mean values were used to plot growth curves and the whisker length represents standard deviation.

Cell adhesion

Log-phage strain cultures were washed with PBS and then resuspended in cell culture medium without antibiotics. Caco-2 cells grown in 24-well plates were infected with the bacterial suspension at an MOI of 10:1. After 45 min, cells were washed three times with PBS to remove the non-attached bacteria and then lysed with 0.1% saponin for 10 min. The number of cell-associated bacteria was determined by plating serial dilutions of the lysate on LB agar plates. The percentage of cell-associated bacteria was calculated as (recovered CFU/inoculated CFU) × 100%, and the results were presented as adhesion relative to wild-type strain (RIMD-W3).

Mouse colonization

Female BALB/c mice aged 6-8 weeks were used to test strain colonization. Mice were randomly divided into three groups, including a control group and two groups inoculated with different strains (three mice each treated group). All mice were fasted for 8 hours prior to gavage.

We introduced plasmids with *lux* reporters (pWHQ205, encoding luciferase and substrate, constructed in this study) into two strains (RIMD-W3 and Δ*puuC*), respectively. Strains carrying *lux* reporters were cultured in LB medium with 3% NaCl supplemented with chloramphenicol (25 μg/ml) to logarithmic phase (OD_{600}=0.6~0.8) at 30°C. Strain concentration was then adjusted to 3×10^{10} CFU/ml with PBS, and each mouse was gavaged with 0.3 ml of the bacterial suspension. At 5 and 10 hours post-infection, the mice were anesthetized with 3% isoflurane for 5 minutes and exposed for 1 minute using the PerkinElmer IVIS Spectrum imaging system (E-Heng Import and Export Co. Ltd).

Mouse lethality

Female BALB/c mice aged 4-5 weeks were used for lethality experiment, which were randomly divided into three groups treated by different strains, with each consisting of 10 mice. Log-phage strain cultures were washed three times with PBS and then adjusted to a concentration of 5×10^{7} CFU/ml with PBS. Mice were intraperitoneally injected with 100 μl of strain suspension, and the number of mice that died at a specific time point was record. The experimental protocols of colonization and lethality of mice were approved by the animal ethics committee of Shanghai Institute of Immunity and Infection (No. A2023011).

Growth competition assay

Log-phage cultures of 12 natural strains, including six wave-1/2/3 and six wave-4 strains (**Supplementary Table 7**), were individually diluted to an OD_{600} of 0.08. Subsequently, the diluted cultures of wave-4 strains were mixed with those of wave-1 to wave-3 strains in equal (1:1) or different (1:5) ratios. Given the ecological relevance of chitin as a major nutrient

source for *Vibrio* spp. in marine environments, and its role as a sole carbon source in aquatic habitats[81], competitions were conducted in natural seawater (collected from Jinshan, Shanghai) supplemented with 0.5% chitin (Sigma). Mixed cultures were incubated at 30 °C under static conditions for 72 h.

Genomic DNA of harvested cultures was extracted using the TIANamp Bacteria DNA kit (Tiangen Biotech). PCR primers VPA0427SNPU (AGCGACGACGCCAGAGAAAG) and VPA0427SNPD (GGTGTCTAAAGTACGGTGCAG) were used to amplify the gene VPA0427, which contains a wave-4 specific SNP allele (A919G). The PCR amplification was performed for 30 cycles, with the parameters: 1) 3 min. at 95°C, 2) 30 sec. at 95°C, 3) 30 sec. at 58°C, 4) 45 sec. at 72°C, 5) repeat steps 2-4 for 30 cycles, 6) 5 min. at 72°C.

The PCR amplification products were used for library construction at Novogene Co. Ltd. (Beijing, China) and sequenced on an Illumina NovaSeq platform. Sequencing reads are trimmed using Trimmomatic v0.39[54] and were then mapped to *V. parahaemolyticus* reference genome using BWA v0.7.17[76]. The frequency of the wave-4 specific allele was calculated to represent the relative abundance of wave-4 strains.

Statistical analysis

Datasets were compared using the Mann-Whitney U test for continuous data and Chi-squared tests for categorical data. Log-rank (Mantel-Cox) tests were used for survival curve comparison. p-values less than 0.05 were considered statistically significant.

Data availability

The sequencing data have been deposited in the NCBI SRA or GenBank database under accession number PRJNA1117214 and PRJNA1062747. Background information of sequenced isolate is listed in Supplementary Table 1-2. Source data are provided with this paper.

References

1. Bonneaud, C. & Longdon, B. Emerging pathogen evolution: Using evolutionary theory to understand the fate of novel infectious pathogens. *EMBO Rep* **21**, (2020).
2. Balasubramanian, D., López-Pérez, M., Grant, T. A., Ogbunugafor, C. B. & Almagro-Moreno, S. Molecular mechanisms and drivers of pathogen emergence. *Trends in Microbiology* vol. 30 Preprint at https://doi.org/10.1016/j.tim.2022.02.003 (2022).
3. Baker-Austin, C. *et al.* Vibrio spp. infections. *Nat Rev Dis Primers* **4**, 8 (2018).
4. Hu, D. *et al.* Origins of the current seventh cholera pandemic. *Proc Natl Acad Sci U S A* **113**, E7730–E7739 (2016).
5. Mutreja, A. *et al.* Evidence for several waves of global transmission in the seventh cholera pandemic. *Nature* **477**, 462–465 (2011).
6. Didelot, X. *et al.* The Role of China in the Global Spread of the Current Cholera Pandemic. *PLoS Genet* **11**, (2015).
7. Weill, F.-X. *et al.* Genomic History of the Seventh Pandemic of Cholera in Africa. Science, , 358: 785-789 (2017).

8. Baker-Austin, C., Stockley, L., Rangdale, R. & Martinez-Urtaza, J. Environmental occurrence and clinical impact of Vibrio vulnificus and Vibrio parahaemolyticus: A European perspective. *Environ Microbiol Rep* **2**, 7–18 (2010).
9. Yang, C. *et al.* Recent mixing of Vibrio parahaemolyticus populations. *ISME J* **13**, 2578–2588 (2019).
10. Nair, G. B. *et al.* Global dissemination of Vibrio parahaemolyticus serotype O3:K6 and its serovariants. *Clin Microbiol Rev* **20**, 39–48 (2007).
11. Espejo, R. T., García, K. & Plaza, N. Insight into the origin and evolution of the Vibrio parahaemolyticus pandemic strain. *Front Microbiol* **8**, 1–6 (2017).
12. Han, D., Yu, F., Chen, X., Zhang, R. & Li, J. Challenges in Vibrio parahaemolyticus infections caused by the pandemic clone. *Future Microbiol* **14**, 437–450 (2019).
13. Matsumoto, C. *et al.* Pandemic spread of an O3:K6 clone of Vibrio parahaemolyticus and emergence of related strains evidenced by arbitrarily primed PCR and toxRS sequence analyses. *J Clin Microbiol* **38**, (2000).
14. Nasu, H. *et al.* A filamentous phage associated with recent pandemic Vibrio parahaemolyticus O3:K6 strains. *J Clin Microbiol* **38**, (2000).
15. Hurley, C. C., Quirke, A. M., Reen, F. J. & Boyd, E. F. Four genomic islands that mark post-1995 pandemic Vibrio parahaemolyticus isolates. *BMC Genomics* **7**, 1–19 (2006).
16. Boyd, E. F. *et al.* Molecular analysis of the emergence of pandemic Vibrio parahaemolyticus. *BMC Microbiol* **8**, 1–14 (2008).
17. Cui, Y. *et al.* Epidemic clones, oceanic gene pools, and eco-LD in the free living marine pathogen vibrio parahaemolyticus. *Mol Biol Evol* **32**, 1396–1410 (2015).
18. Sela, I., Wolf, Y. I. & Koonin, E. V. Theory of prokaryotic genome evolution. *Proc Natl Acad Sci U S A* **113**, 11399–11407 (2016).
19. Luo, H. How Big Is Big? The Effective Population Size of Marine Bacteria. *Ann Rev Mar Sci* **17**, 537–560 (2025).
20. Liu, Z., Hossain, S. S., Moreira, Z. M. & Haney, C. H. Putrescine and Its Metabolic Precursor Arginine Promote Biofilm and c-di-GMP Synthesis in Pseudomonas aeruginosa. *J Bacteriol* **204**, (2022).
21. Kline, K. A., Fälker, S., Dahlberg, S., Normark, S. & Henriques-Normark, B. Bacterial Adhesins in Host-Microbe Interactions. *Cell Host and Microbe* vol. 5 Preprint at https://doi.org/10.1016/j.chom.2009.05.011 (2009).
22. Yang, C. *et al.* Outbreak dynamics of foodborne pathogen Vibrio parahaemolyticus over a seventeen year period implies hidden reservoirs. *Nat Microbiol* **7**, 1221–1229 (2022).
23. Datta, M. S. *et al.* Rapid methicillin resistance diversification in Staphylococcus epidermidis colonizing human neonates. *Nat Commun* **12**, (2021).
24. Iwasaki, W. & Takagi, T. Rapid pathway evolution facilitated by horizontal gene transfers across prokaryotic lineages. *PLoS Genet* **5**, (2009).
25. Domman, D. *et al.* Integrated View of Vibrio Cholerae in the Americas. Science **358**, 789-793 (2017).
26. Cui, Y. *et al.* Historical variations in mutation rate in an epidemic pathogen, Yersinia pestis. *Proceedings of the National Academy of Sciences* **110**, 577–582 (2013).
27. Rabosky, D. L. & Lovette, I. J. Explosive evolutionary radiations: Decreasing speciation or increasing extinction through time? *Evolution (N Y)* **62**, (2008).

28. Morlon, H., Kemps, B. D., Plotkin, J. B. & Brisson, D. Explosive radiation of a bacterial species group. *Evolution (N Y)* **66**, (2012).
29. Markov, P. V. *et al*. The evolution of SARS-CoV-2. *Nature Reviews Microbiology* **21** (2023).
30. Flemming, H. C. *et al.* Biofilms: An emergent form of bacterial life. *Nature Reviews Microbiology* **14** (2016).
31. Wunderlichová, L., Buňková, L., Koutný, M., Jančová, P. & Buňka, F. Formation, Degradation, and Detoxification of Putrescine by Foodborne Bacteria: A Review. *Compr Rev Food Sci Food Saf* **13**, (2014).
32. Krammer, E. M. & Prévost, M. Function and Regulation of Acid Resistance Antiporters. *Journal of Membrane Biology* **252**, (2019).
33. Romano, A., Ladero, V., Alvarez, M. A. & Lucas, P. M. Putrescine production via the ornithine decarboxylation pathway improves the acid stress survival of Lactobacillus brevis and is part of a horizontally transferred acid resistance locus. *Int J Food Microbiol* **175**, (2014).
34. Hohmann, A. W., Schmidt, G. & Rowley, D. Intestinal colonization and virulence of Salmonella in mice. *Infect Immun* **22**, (1978).
35. Wang, Y. *et al.* Isolation, phylogenetic group, drug resistance, biofilm formation, and adherence genes of Escherichia coli from poultry in central China. *Poult Sci* **95**, (2016).
36. Flament-Simon, S. C. *et al.* Association between kinetics of early biofilm formation and clonal lineage in Escherichia coli. *Front Microbiol* **10**, (2019).
37. Hogins, J., Xuan, Z., Zimmern, P. E. & Reitzer, L. The distinct transcriptome of virulence-associated phylogenetic group B2 Escherichia coli . *Microbiol Spectr* **11**, (2023).
38. Nowrouzian, F. L., Wold, A. E. & Adlerberth, I. Escherichia coli strains belonging to phylogenetic group B2 have superior capacity to persist in the intestinal microflora of infants. *Journal of Infectious Diseases* **191**, (2005).
39. Grozdanov, L. *et al.* Analysis of the genome structure of the nonpathogenic probiotic Escherichia coli strain Nissle 1917. *J Bacteriol* **186**, (2004).
40. Chattaway, M. A., Schaefer, U., Tewolde, R., Dallman, T. J. & Jenkins, C. Identification of Escherichia coli and shigella species from whole-genome sequences. *J Clin Microbiol* **55**, (2017).
41. Viana, D. *et al.* A single natural nucleotide mutation alters bacterial pathogen host tropism. *Nat Genet* **47**, (2015).
42. Arnold, B. J., Huang, I. T. & Hanage, W. P. Horizontal gene transfer and adaptive evolution in bacteria. *Nature Reviews Microbiology* **20** 206–218 (2022).
43. Rodríguez-Beltrán, J., DelaFuente, J., León-Sampedro, R., MacLean, R. C. & San Millán, Á. Beyond horizontal gene transfer: the role of plasmids in bacterial evolution. *Nature Reviews Microbiology* **19** 347–359 (2021).
44. Albalat, R. & Cañestro, C. Evolution by gene loss. *Nature Reviews Genetics* **17** 379–391 (2016).
45. Wolf, Y. I. & Koonin, E. V. Genome reduction as the dominant mode of evolution. *BioEssays* **35**, (2013).
46. Pallen, M. J. & Wren, B. W. Bacterial pathogenomics. *Nature* **449**, 835–842 (2007).
47. McCutcheon, J. P. & Moran, N. A. Extreme genome reduction in symbiotic bacteria.

Nature Reviews Microbiology **10** 13–26 (2012).

48. Maurelli, A. T., Fernández, R. E., Bloch, C. A., Rode, C. K. & Fasano, A. “Black holes” and bacterial pathogenicity: A large genomic deletion that enhances the virulence of *Shigella* spp. and enteroinvasive *Escherichia coli*. *Proc Natl Acad Sci U S A* **95**, 3943–3948 (1998).
49. Maurelli, A. T. Black holes, antivirulence genes, and gene inactivation in the evolution of bacterial pathogens. *FEMS Microbiology Letters* **267** (2007).
50. Bliven, K. A. & Maurelli, A. T. Antivirulence genes: Insights into pathogen evolution through gene loss. *Infection and Immunity* **80** 4061–4070 (2012).
51. Dufresne, A., Garczarek, L. & Partensky, F. Accelerated evolution associated with genome reduction in a free-living prokaryote. *Genome Biol* **6**, (2005).
52. Morris, J. J., Lenski, R. E. & Zinser, E. R. The black queen hypothesis: Evolution of dependencies through adaptive gene loss. *mBio* **3**, (2012).
53. Alizon, S., Hurford, A., Mideo, N. & Van Baalen, M. Virulence evolution and the trade-off hypothesis: History, current state of affairs and the future. *Journal of Evolutionary Biology* **22** (2009).
54. Bolger, A. M., Lohse, M. & Usadel, B. Trimmomatic: a flexible trimmer for Illumina sequence data. *Bioinformatics* **30**, 2114–2120 (2014).
55. Parks, D. H., Imelfort, M., Skennerton, C. T., Hugenholtz, P. & Tyson, G. W. CheckM: Assessing the quality of microbial genomes recovered from isolates, single cells, and metagenomes. *Genome Res* **25**, 1043–1055 (2015).
56. Jain, C., Rodriguez-R, L. M., Phillippy, A. M., Konstantinidis, K. T. & Aluru, S. High throughput ANI analysis of 90K prokaryotic genomes reveals clear species boundaries. *Nat Commun* **9**, 1–8 (2018).
57. Delcher, A. L., Salzberg, S. L. & Phillippy, A. M. Using MUMmer to Identify Similar Regions in Large Sequence Sets . *Curr Protoc Bioinformatics* **00**, (2003).
58. Page, A. J. *et al.* SNP-sites: rapid efficient extraction of SNPs from multi-FASTA alignments. *Microb Genom* **2**, e000056 (2016).
59. Benson, G. Tandem repeats finder: a program to analyze DNA sequences. *Nucleic Acids Res* **27**, 573–580 (1999).
60. Price, M. N., Dehal, P. S. & Arkin, A. P. FastTree 2 – Approximately Maximum-Likelihood Trees for Large Alignments. *PLoS One* **5**, e9490 (2010).
61. Croucher, N. J. *et al.* Rapid phylogenetic analysis of large samples of recombinant bacterial whole genome sequences using Gubbins. *Nucleic Acids Res* **43**, e15 (2015).
62. Edwards, D., Duchêne, S., Pope, B. & Holt, K. SNPPar: identifying convergent evolution and other homoplasies from microbial whole-genome alignments. **264017**, 1–33 (2020).
63. Kozlov, A. M. *et al.* RAxML-NG: A fast, scalable and user-friendly tool for maximum likelihood phylogenetic inference. *Bioinformatics* (2019).
64. Yu, G., Smith, D. K., Zhu, H., Guan, Y. & Lam, T. T. Y. ggtree: an r package for visualization and annotation of phylogenetic trees with their covariates and other associated data. *Methods Ecol Evol* **8**, (2017).
65. Tonkin-Hill, G., Lees, J. A., Bentley, S. D., Frost, S. D. W. & Corander, J. Fast hierarchical Bayesian analysis of population structure. *Nucleic Acids Res* **47**, 5539–5549 (2019).
66. Rambaut, A., Lam, T. T., Carvalho, L. M. & Pybus, O. G. Exploring the temporal structure

of heterochronous sequences using TempEst (formerly Path-O-Gen). *Virus Evol* **2**, (2016).

67. Didelot, X., Croucher, N. J., Bentley, S. D., Harris, S. R. & Wilson, D. J. Bayesian inference of ancestral dates on bacterial phylogenetic trees. *Nucleic Acids Res* **46**, (2018).

68. Volz, E. M. & Didelot, X. Modeling the growth and decline of pathogen effective population size provides insight into epidemic dynamics and drivers of antimicrobial resistance. *Syst Biol* **67**, 719–728 (2018).

69. van der Graaf-Van Bloois, L., Chen, H., Wagenaar, J. A. & Zomer, A. L. Development of Kaptive databases for Vibrio parahaemolyticus O-and K-antigen genotyping. *Microb Genom* **9**, (2023).

70. Seemann, T. Prokka: rapid prokaryotic genome annotation. *Bioinformatics* **30**, 2068–2069 (2014).

71. Tonkin-Hill, G. *et al.* Producing polished prokaryotic pangenomes with the Panaroo pipeline. *Genome Biol* **21**, 180 (2020).

72. Parks, D. H. *et al.* GTDB: An ongoing census of bacterial and archaeal diversity through a phylogenetically consistent, rank normalized and complete genome-based taxonomy. *Nucleic Acids Res* **50**, D785–D794 (2022).

73. Chimalapati, S., Lafrance, A. E., Chen, L. & Orth, K. Vibrio parahaemolyticus: Basic Techniques for Growth, Genetic Manipulation, and Analysis of Virulence Factors. *Curr Protoc Microbiol* **59**, (2020).

74. Datsenko, K. A. & Wanner, B. L. One-step inactivation of chromosomal genes in Escherichia coli K-12 using PCR products. *Proc Natl Acad Sci U S A* **97**, (2000).

75. Sharma, C. M., Darfeuille, F., Plantinga, T. H. & Vogel, J. A small RNA regulates multiple ABC transporter mRNAs by targeting C/A-rich elements inside and upstream of ribosome-binding sites. *Genes Dev* **21**, (2007).

76. Li, H. & Durbin, R. Fast and accurate short read alignment with Burrows-Wheeler transform. *Bioinformatics* **25**, 1754–1760 (2009).

77. Liao, Y., Smyth, G. K. & Shi, W. FeatureCounts: An efficient general purpose program for assigning sequence reads to genomic features. *Bioinformatics* **30**, (2014).

78. Love, M. I., Huber, W. & Anders, S. Moderated estimation of fold change and dispersion for RNA-seq data with DESeq2. *Genome Biol* **15**, (2014).

79. Wu, T. *et al.* clusterProfiler 4.0: A universal enrichment tool for interpreting omics data. *The Innovation* **2**, 100141 (2021).

80. Zhou, H. *et al.* Characterization of a natural triple-tandem c-di-GMP riboswitch and application of the riboswitch-based dual-fluorescence reporter. *Sci Rep* **6**, (2016).

81. Meiborn, K. L. *et al.* The Vibrio cholerae chitin utilization program. *Proc Natl Acad Sci U S A* **101**, (2004).

Acknowledgements

This work was supported by National Key Research and Development Program of China (No. 2022YFC2304700 to F.D.), National Natural Science Foundation of China (No. 32270003 and No. 32000008 to C.Y., No. 32170640 and No.32211550014 to D.F., No. 32250610209 to S.S.), Youth Innovation Promotion Association, Chinese Academy of Sciences (No. 2022278 to C.Y.), Ministerio de Ciencia e Innovación (Spain) Grant PID2021-127107NB-I00 (J.M.U.), Generalitat de Catalunya Grant 2021 SGR 00526 (J.M.U.), Shanghai Rising-Star Program (No. 23QA1410500 to C.Y.), Shanghai Public Health System Construction Three-Year Action Plan (No. GWVI-11.1-43 to H.Q.) and Wuxi Science and Technology Development Fund's

'Light of Taihu Lake' Science and Technology Research Program (Basic Research) (No. K20231033 to C.N., No. K20231045 to S.G.). We are grateful to the labs of Prof. Qiyao Wang, Kim Orth, and Jin He for providing strains and plasmids. We thank Prof. Lei Pan for valuable comments.

Author contributions

C.Y., J.M.-U. and D.F. designed, initiated and coordinated the study. J.M.-U., L.X, Y.L., M.J., X.S. and Q.H. contributed to data collection. C.Y., Z.J., J.W., and W.X. performed bioinformatics analysis. H.Q, S.S., C.N., S.G., Z.J., H.W., Y.Q. and S.L. performed experiments. All authors contributed to interpretation of the data. C.Y. wrote the first draft of the paper and H.Q., S.S., Y.Z., Z.Z., Y.C., J.M.-U., H.W., R.Y., Y.C. and D.F. reviewed and revised the paper. All authors read and approved the final manuscript.

Competing interests

The authors declare no competing interests.

Figure legends

Figure 1. From pre-pandemic (pre-PC) to pandemic clone (PC). a) Maximum likelihood tree of 8,684 global isolates. Pre-PC and PC isolates are colored in blue and red, respectively. b) Inferred evolutionary history from pre-PC to PC. The status of known PC marker genes/islands in the ancestral strain is indicated by blue ellipses, while subsequent gains or losses are represented by orange and black triangles. The numbers next to tree nodes indicate inferred divergence times and 95% confidence intervals. Dashed lines represent lineages with unknown origination times due to a lack of significant temporal signal. c) Distribution of virulence-associated loci and known PC marker genes/islands among pre-PC, PC and non-PC strains. Double slashes indicate artificially shortened phylogenetic branches. Heatmap fill colors represent the frequency of presence for each locus across groups.

Figure 2. Fine-scale population structure, spatiotemporal and population dynamics of PC. a) Maximum likelihood tree of 942 representative PC strains. The colors represent different waves. Double slashes indicate artificially truncated branches. b) Dated phylogeny of PC (left) and the geographical, subtyping and distribution of genes in the putrescine utilization (Puu) pathway of strains (right). The colors of tree branches indicate geographic areas, and numbers next to tree nodes indicate inferred divergence times and 95% confidence intervals. TCs indicate transmissions resulting in local colonization. (c) Temporal dynamics of four waves. Bar colors indicate the frequency of different waves. The line represents the number of representative strains. (d) Temporal distribution of representative strains in different countries and regions. The size of circles scales with the number of representative strains. (e) Effective population size dynamics of different waves of the PC.

Figure 3. Effect of gene-loss in putrescine utilization (Puu) pathway. a) Positions of wave-4 specific variations on the reference genome (top) and gene structure and coverage of Puu-genes (colored in blue) in different waves (bottom). b) Summary of Puu-genes and metabolites based on KEGG annotations. The *puuC* gene, which appears in three sub-pathway, was highlighted in bold. c) Biofilm levels in M9 minimal media with 1% NaCl measured by optical density at 595 nm (OD_{595}) of wildtype (RIMD-W3), mutant (Δ*puuC*) and complement strains (C-Δ*puuC*). d) Transcriptomic volcano plots showing differentially expressed genes (DEGs). The colors represent genes of specific category as in the legend. Red and blue backgrounds represent up- and down-regulated genes in Δ*puuC* compared to wildtype strain. e) c-di-GMP dynamics of wildtype (RIMD-W3) and mutant (Δ*puuC*) strains. f) The adhesion ability of strains to Caco-2 cells relative to wildtype (RIMD-W3). g) *In vivo* bioluminescent imaging of mice at 5 hours post-infection by gavage. h) Survival curves of mice by intraperitoneal infection. Mann-Whitney U test was used for pairwise comparisons except for panel h, where log-rank (Mantel-Cox) tests were applied. *: $p<0.05$, **: $p<0.01$.

Figure 4. Phenotypes and clinical symptoms of wave1-3 and wave-4 strains. a) Biofilm level and adhesion ability between wave1-3 and wave-4 strains. b) Biofilm level and adhesion ability between the wave-4 wildtype strain (VPCZ58, wave-4 WT) and its complemented strain (wave-4 WT C-(VP1775-1786)) carrying the nine puu-related genes (VP1775-1786). c) Clinical symptoms of wave-4 and other wave-associated patients. d) Wave-4 specific allele

frequency after 72 hours of competition under seawater with chitin conditions. The light blue and dark blue bars represent the mixture of natural strains before and after competition, respectively. The Mann-Whitney U test was used for pairwise comparisons, except for panel c, where Chi-squared tests were applied. *: $p<0.05$, **: $p<0.01$.

Figure 5. Puu-genes in 36 bacterial species. a) Prevalence of Puu-genes in 36 species. Genes and sub-pathways (SP) on the left are as in Fig. 3b. The colors (right) indicate the frequency of genes. b) Phylogenetic distribution of Puu-genes in 10 species and the biofilm and adhesion of wildtype (E7946 and MG1655) and Δ*puuC* mutant strains in *V. cholerae* and *E. coli*. Mann-Whitney U test was used for pairwise comparisons. *: $p<0.05$, **: $p<0.01$.

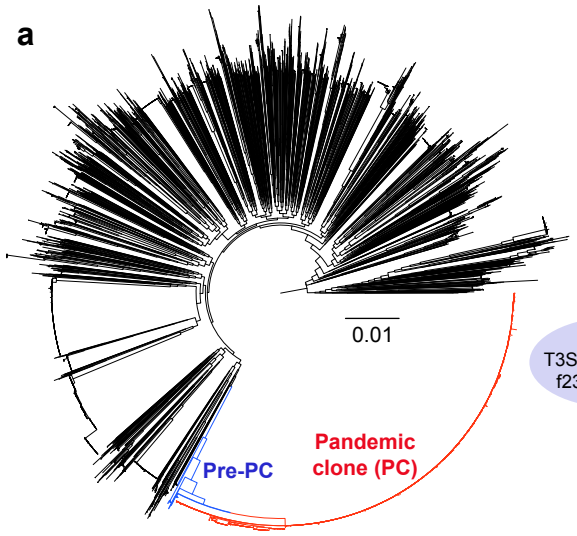
a
0.01
Pre-PC
Pandemic
clone (PC)

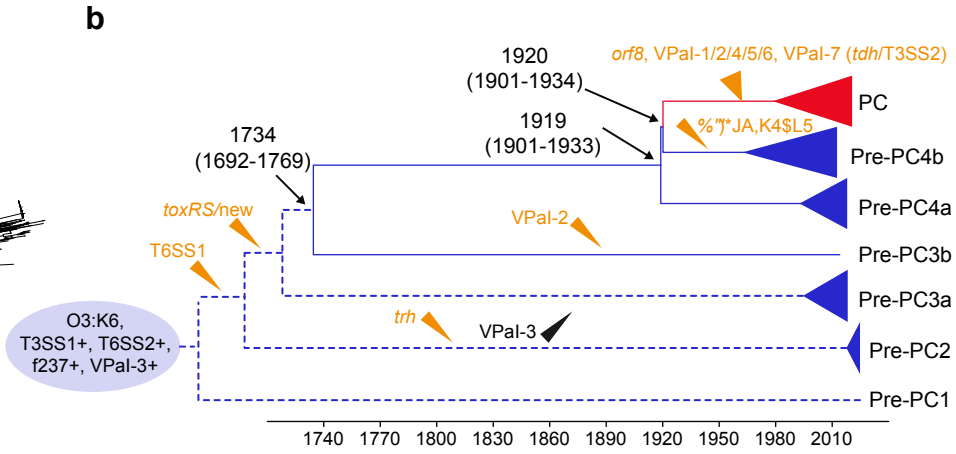
b
1920
(1901-1934)
orf8, VPaI-1/2/4/5/6, VPaI-7 (tdh/T3SS2)
PC
1919
(1901-1933)
%"}*JA,K4$L5
Pre-PC4b
1734
(1692-1769)
toxRS/new
Pre-PC4a
VPaI-2
T6SS1
Pre-PC3b
O3:K6,
T3SS1+, T6SS2+,
f237+, VPaI-3+
Pre-PC3a
trh
VPaI-3
Pre-PC2
Pre-PC1
1740 1770 1800 1830 1860 1890 1920 1950 1980 2010

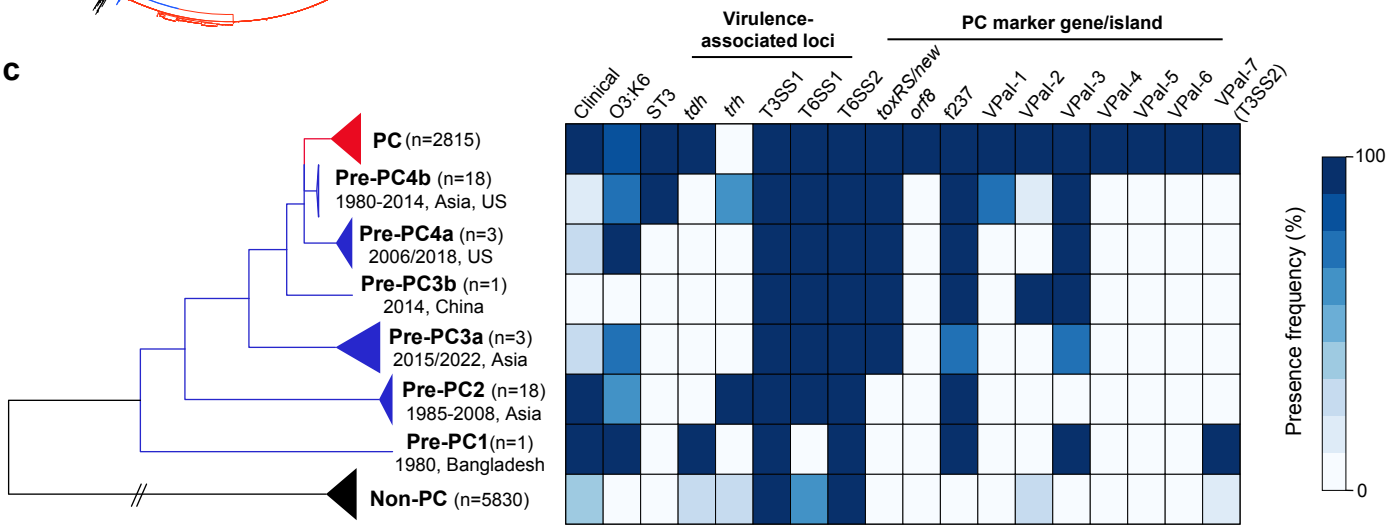
c
PC (n=2815)
Pre-PC4b (n=18)
1980-2014, Asia, US
Pre-PC4a (n=3)
2006/2018, US
Pre-PC3b (n=1)
2014, China
Pre-PC3a (n=3)
2015/2022, Asia
Pre-PC2 (n=18)
1985-2008, Asia
Pre-PC1 (n=1)
1980, Bangladesh
Non-PC (n=5830)
Virulence-associated loci
PC marker gene/island
Clinical
O3:K6
ST3
tdh
trh
T3SS1
T6SS1
T6SS2
toxRS/new
orf8
f237
VPaI-1
VPaI-2
VPaI-3
VPaI-4
VPaI-5
VPaI-6
VPaI-7 (T3SS2)
Presence frequency (%)
100
0

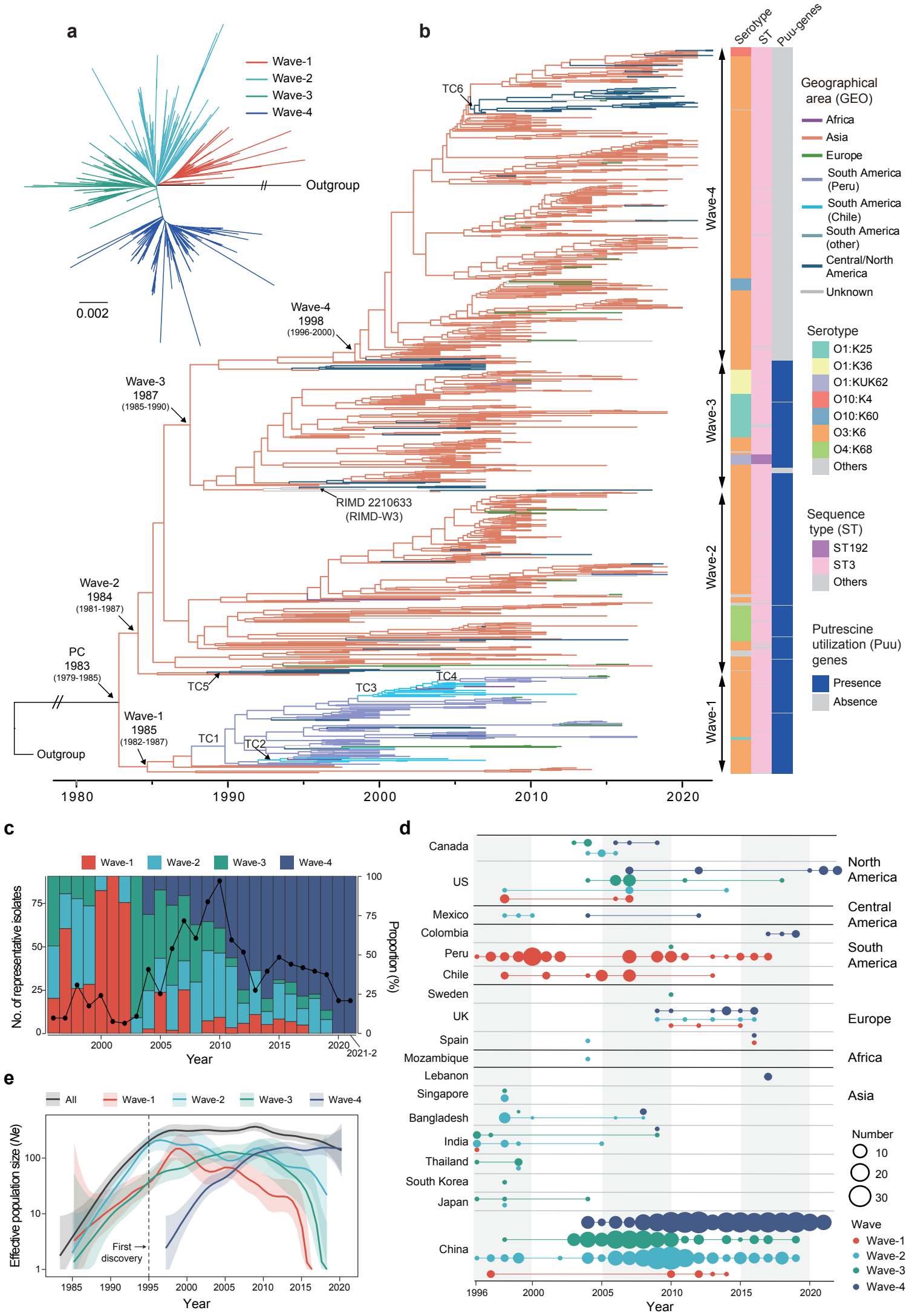
a
Wave-1
Wave-2
Wave-3
Wave-4
Outgroup
0.002
b
Serotype
ST
Puu-genes
TC6
Wave-4
1998
(1996-2000)
Wave-3
1987
(1985-1990)
RIMD 2210633
(RIMD-W3)
Wave-2
1984
(1981-1987)
PC
1983
(1979-1985)
TC5
TC4
TC3
Wave-1
1985
(1982-1987)
TC1
TC2
Outgroup
1980
1990
2000
2010
2020
Geographical area (GEO)
Africa
Asia
Europe
South America (Peru)
South America (Chile)
South America (other)
Central/North America
Unknown
Serotype
O1:K25
O1:K36
O1:KUK62
O10:K4
O10:K60
O3:K6
O4:K68
Others
Sequence type (ST)
ST192
ST3
Others
Putrescine utilization (Puu) genes
Presence
Absence
c
Wave-1
Wave-2
Wave-3
Wave-4
No. of representative isolates
Proportion (%)
Year
2021-2
d
Canada
US
Mexico
Colombia
Peru
Chile
Sweden
UK
Spain
Mozambique
Lebanon
Singapore
Bangladesh
India
Thailand
South Korea
Japan
China
North America
Central America
South America
Europe
Africa
Asia
Number
10
20
30
Wave
Wave-1
Wave-2
Wave-3
Wave-4
Year
e
All
Wave-1
Wave-2
Wave-3
Wave-4
Effective population size (Ne)
First discovery
Year

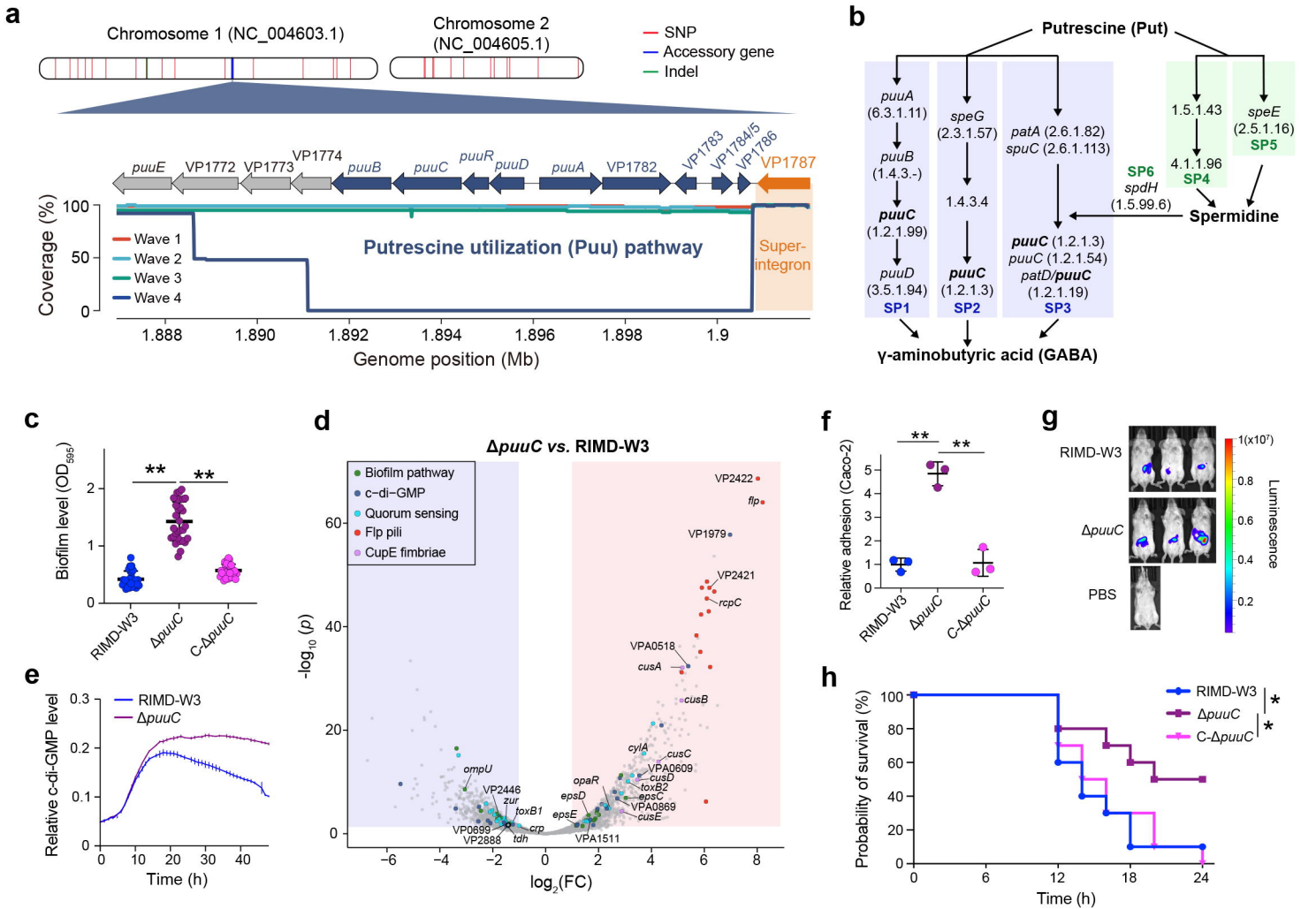
a
Chromosome 1 (NC_004603.1)
Chromosome 2 (NC_004605.1)
SNP
Accessory gene
Indel
puuE
VP1772
VP1773
VP1774
puuB
puuC
puuR
puuD
puuA
VP1782
VP1783
VP1784/5
VP1786
VP1787
Coverage (%)
Wave 1
Wave 2
Wave 3
Wave 4
Putrescine utilization (Puu) pathway
Super-integron
Genome position (Mb)
b
Putrescine (Put)
puuA (6.3.1.11)
puuB (1.4.3.-)
puuC (1.2.1.99)
puuD (3.5.1.94)
SP1
speG (2.3.1.57)
1.4.3.4
puuC (1.2.1.3)
SP2
patA (2.6.1.82)
spuC (2.6.1.113)
puuC (1.2.1.3)
puuC (1.2.1.54)
patD/puuC (1.2.1.19)
SP3
1.5.1.43
4.1.1.96
SP4
speE (2.5.1.16)
SP5
SP6
spdH (1.5.99.6)
Spermidine
γ-aminobutyric acid (GABA)
c
Biofilm level (OD595)
RIMD-W3
ΔpuuC
C-ΔpuuC
d
ΔpuuC vs. RIMD-W3
Biofilm pathway
c-di-GMP
Quorum sensing
Flp pili
CupE fimbriae
-log10 (p)
log2(FC)
VP2422
flp
VP1979
VP2421
rcpC
VPA0518
cusA
cusB
cylA
cusC
VPA0609
cusD
toxB2
epsC
VPA0869
cusE
opaR
epsD
epsE
VPA1511
ompU
VP2446
zur
toxB1
crp
tdh
VP0699
VP2888
e
Relative c-di-GMP level
RIMD-W3
ΔpuuC
Time (h)
f
Relative adhesion (Caco-2)
RIMD-W3
ΔpuuC
C-ΔpuuC
g
RIMD-W3
ΔpuuC
PBS
Luminescence
h
Probability of survival (%)
RIMD-W3
ΔpuuC
C-ΔpuuC
Time (h)

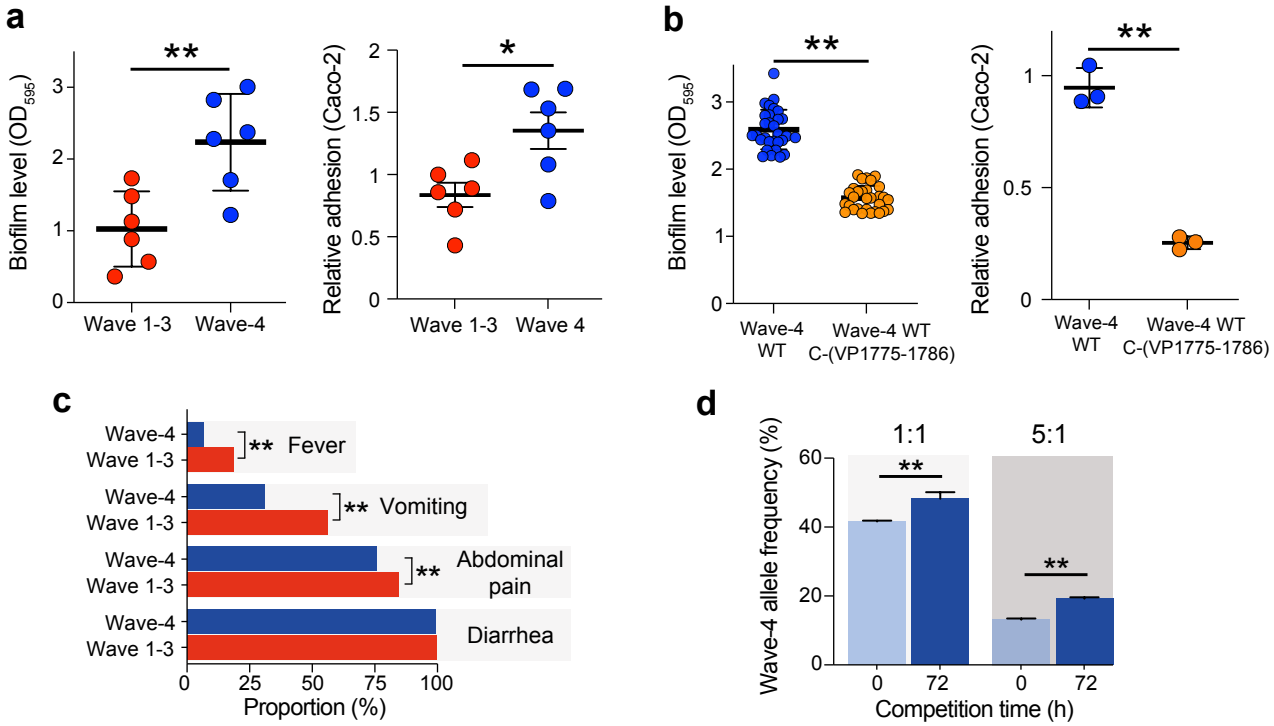
a
Biofilm level (OD595)
**
Wave 1-3
Wave-4
Relative adhesion (Caco-2)
*
Wave 1-3
Wave 4
b
Biofilm level (OD595)
**
Wave-4 WT
Wave-4 WT C-(VP1775-1786)
Relative adhesion (Caco-2)
**
Wave-4 WT
Wave-4 WT C-(VP1775-1786)
c
Wave-4
Wave 1-3
** Fever
** Vomiting
** Abdominal pain
Diarrhea
Proportion (%)
d
1:1
5:1
Wave-4 allele frequency (%)
**
**
Competition time (h)

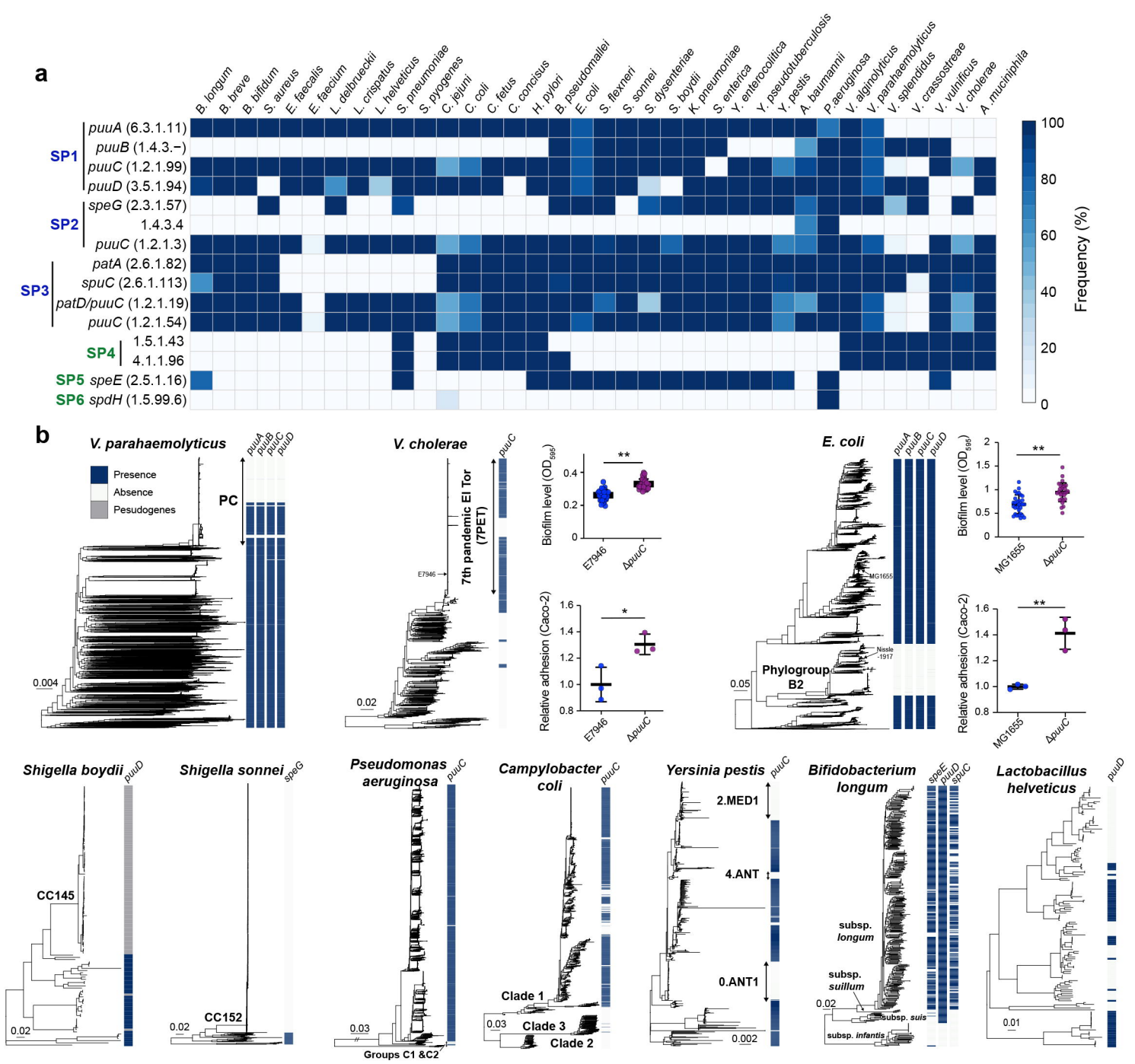
a
B. longum
B. breve
B. bifidum
S. aureus
E. faecalis
E. faecium
L. delbrueckii
L. crispatus
L. helveticus
S. pneumoniae
S. pyogenes
C. jejuni
C. coli
C. fetus
C. concisus
H. pylori
B. pseudomallei
E. coli
S. flexneri
S. sonnei
S. dysenteriae
S. boydii
K. pneumoniae
S. enterica
Y. enterocolitica
Y. pseudotuberculosis
Y. pestis
A. baumannii
P. aeruginosa
V. alginolyticus
V. parahaemolyticus
V. splendidus
V. crassostreae
V. vulnificus
V. cholerae
A. muciniphila
SP1
puuA (6.3.1.11)
puuB (1.4.3.–)
puuC (1.2.1.99)
puuD (3.5.1.94)
SP2
speG (2.3.1.57)
1.4.3.4
puuC (1.2.1.3)
SP3
patA (2.6.1.82)
spuC (2.6.1.113)
patD/puuC (1.2.1.19)
puuC (1.2.1.54)
SP4
1.5.1.43
4.1.1.96
SP5 speE (2.5.1.16)
SP6 spdH (1.5.99.6)
Frequency (%)
100
80
60
40
20
0
b
V. parahaemolyticus
Presence
Absence
Pesudogenes
PC
puuA
puuB
puuC
puuD
0.004
V. cholerae
7th pandemic El Tor (7PET)
E7946
0.02
Biofilm level (OD595)
Relative adhesion (Caco-2)
E7946
ΔpuuC
E. coli
MG1655
Nissle -1917
Phylogroup B2
0.05
Shigella boydii
CC145
0.02
Shigella sonnei
CC152
0.02
Pseudomonas aeruginosa
0.03
Groups C1 &C2
Campylobacter coli
Clade 1
Clade 3
Clade 2
0.03
Yersinia pestis
2.MED1
4.ANT
0.ANT1
0.002
Bifidobacterium longum
subsp. longum
subsp. suillum
subsp. suis
subsp. infantis
speE
spuC
0.02
Lactobacillus helveticus
0.01